# Three-Dimensional Computer Simulation in Deep Regional Hyperthermia Using the Finite-Difference Time-Domain Method

DENNIS SULLIVAN

*Abstract* — **The finite-difference time-domain method is used for detailed three-dimensional simulation for applications in deep regional hyperthermia. The ability to simulate *SAR* patterns from the near field of prototype applicators is demonstrated by comparison with measured data. The method is also used to simulate treatments on commercially available equipment by using a detailed model of a cancer patient constructed from computerized axial tomography scans. The model has 1 cm resolution and consists of 34 751 cells. The method is further used to anticipate results of treatments with prototype applicators.**

## I. Introduction

In the field of radio frequency (RF) hyperthermia, computer simulation has been used to some extent for device evaluation or for anticipating the effectiveness of a treatment. Most simulation techniques have been two-dimensional [1]–[3]. Recently, more realistic three-dimensional modeling has begun to appear [4], [5]. In this paper, the finite-difference time-domain (FDTD) method [6] is used as a means of obtaining realistic three-dimensional simulations in several phases of deep regional hyperthermia: new applicator design, treatment planning, and comparison of prototype applicators with commercially available equipment.

Thus far, no completely acceptable method is available to selectively heat deep-seated cancer tumors. The annular phased array (APA) [7], [8] is presently the most widely used method. The APA concept employs a group of aperture or dipole applicators arranged in an annulus. The patient is positioned in the annular opening. It is hoped that the configuration of the applicators will result in constructive interference of the dominant $E$ field within the patient. Such a method involves the use of large amounts of power, which heat good tissue as well as tumor. The resulting stress and pain to the patient often prevent the completion of a satisfactory treatment. Recent developments offer the possibility of steering the peak of the $E$ fields by manipulating the amplitude and phase of the individual applicators [2], [4]. However, the very complex fields that result within an inhomogeneous human body will invariably hinder such an approach.

An attractive alternative to a fixed annular array is the use of several discrete applicators, which could be placed on the patient in such a way that the energy would be more effectively directed to the tumor site. Such a method might result in less net power deposited in good tissue; hopefully, therapeutic temperatures within the tumor could be achieved with less stress to the patient. The disadvantage to such a method is the increased possibility of skin or outer tissue burns at the site of the applicator.

The development of new applicators is hindered by the fact that the body being treated is in the near field of the applicator, which affects the performance of the applicator itself. This makes the predicted performance of a new applicator by analytic methods almost impossible. Repeated construction and testing of new applicators by trial and error are time consuming and expensive.

This paper presents the possibility of using computer simulation to design new applicators. Using Cray XMP and Cray II supercomputers, the FDTD method is used to predict the detailed near field of RF applicators. Prototypes have been built, and good correlation has been found between predicted and measured specific absorption rate ($SAR$) distribution.

In addition, this same method is demonstrated for use in treatment planning. Using data from computerized axial tomography (CAT) scans of cancer patients, a treatment using a commercially available device, the Sigma-60 applicator of the BSD-2000 Hyperthermia System, can be simulated. For comparison, a treatment using the new prototype applicators can also be simulated.

## II. Description of the Method

The method used to calculate the EM fields from RF applicators is the FDTD method. FDTD is a time-domain method which positions the $\boldsymbol{E}$ and $\boldsymbol{H}$ vectors around a unit cell (Fig. 1), a concept first proposed by Yee [9]. The addition of radiation boundary conditions [10] and sinusoidal wave source/observation conditions [11], [12] made this a computationally efficient means to calculate EM wave interactions with arbitrary structures. It has been used extensively to calculate scattering from metallic ob-

Manuscript received April 28, 1989; revised September 19, 1989. This work was supported by NCI grants CA 40434 and CA 44664 and by grants for computer time from the San diego Supercomputer Center and from the Numerical Aerodynamic Simulation Program of the National Aeronautics and Space Administration.

The author is with the Department of Radiation Oncology, Stanford University School of Medicine, Stanford, CA 94305.

IEEE Log Number 8932004.

0018-9480/90/0200-0204$01.00 ©1990 IEEE

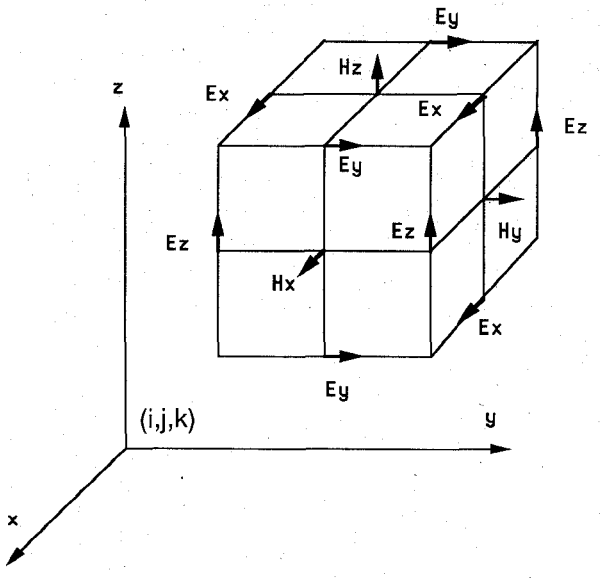


Fig. 1. Position of the field components about a unit cell of the lattice.

jects. Specifically, the U.S. Department of Defense has funded studies to determine nuclear EM pulse interaction with missiles and aircraft [12], [13]. Although it had seen some use in calculating EM energy absorption [14], it is only with the advent of supercomputers that detailed calculation of the EM absorption of a human body exposed to a microwave field has become possible, i.e., bodies modeled by 5000 cells or more [15], [16].

The FDTD method is a straightforward implementation of the time-dependent Maxwell's equations:

$$\epsilon\frac{\delta \boldsymbol{E}}{\delta t}+\boldsymbol{J}=\nabla\times\boldsymbol{H} \qquad -\frac{\delta \boldsymbol{B}}{\delta t}=\nabla\times\boldsymbol{E}. \tag{1}$$

These vector equations can be written as six separate partial differential equations, one of which is

$$\frac{\partial E_z}{\partial t}=\frac{1}{\epsilon}\left(\frac{\partial H_y}{\partial x}-\frac{\partial H_x}{\partial y}-\sigma E_z\right). \tag{2}$$

This, in turn, can be written as a difference equation for implementation on a computer:

$$EZ(I,J,K)=CAZ(I,J,K)*EZ(I,J,K)+$$
$$CBZ(I,J,K)*[HY(I,J,K)-HY(I-1,J,K)$$
$$+HX(I,J-1,K)-HX(I,J,K)] \tag{3}$$

where $I, J, K$ represent position in the $x$, $y$, and $z$ directions, $EZ$, $HX$, and $HY$ represent the $E_z$, $H_x$, and $H_y$ fields, and $CAZ$ and $CBZ$ are parameters determined by frequency, cell size, and the electromagnetic characteristics of the material at point $I, J, K$. Five similar equations are needed for the full representation of Maxwell's equations. It is assumed that the $\boldsymbol{E}$ and $\boldsymbol{H}$ vectors are positioned around a unit cell (Fig. 1) and that the collection of these cells form the three-dimensional lattice that contains the problem being simulated. All the simulations reported in this paper used a cell size of 1 cm. (Details of the method are well documented and will not be repeated here [4], [11], [12], [15].) The method is particularly suitable for processing on a supercomputer, because the difference equations take full advantage of the vectorizing capability.

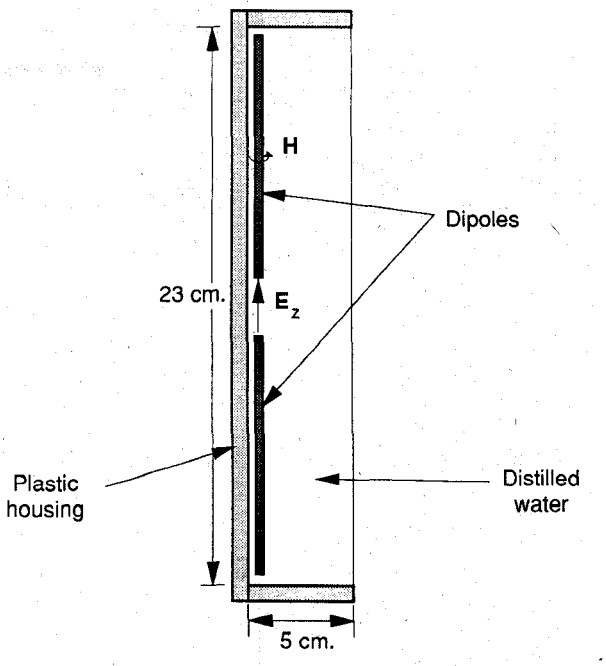


Fig. 2. Dipole applicator. The width, perpendicular to the plane of the paper, is 9 cm.

## III. Applicator Design

In this section are shown the results of tests to determine the ability of the FDTD method to accurately predict the $SAR$ pattern of an applicator in close proximity to a biological body. The applicator used was a simple dipole in a plastic housing containing distilled water (Fig. 2). Since the dipole is next to the back wall of the applicator, the dipole is loaded to one side by water and the other side by air. Because the lengths of the dipoles used are selected to be on the order of a half or a whole wavelength in water, the majority of the power goes out the front of the applicator. The electrical stimulation of the dipole is simulated by assigning the gap between the arms the values

$$E_z=\sin(2\cdot\pi\cdot n\cdot\delta t) \tag{4}$$

where $\delta t$ is the time increment, and $n=1,2,\cdots,NMAX$ with $NMAX$ being the number of iterations needed to get a steady-state solution.

As the Maxwell equations of (1) are solved, the $E$ and $H$ fields are propagated through the problem space. Typically, steady state is reached after three to five wavelengths. The $SAR$ is determined in the following manner. As the $E$ fields are being propagated, all three $E$ fields are being monitored at every cell in the problem space for positive and negative peaks. When a peak is reached, that value is saved. The $SAR$ is then calculated from

$$SAR(i,j,k)=\frac{1}{2}*\sigma(i,j,k)$$
$$*\left(E_x^2(i,j,k)+E_y^2(i,j,k)+E_z^2(i,j,k)\right) \tag{5}$$

where $E_x$, $E_y$, and $E_z$ are calculated from the positive and

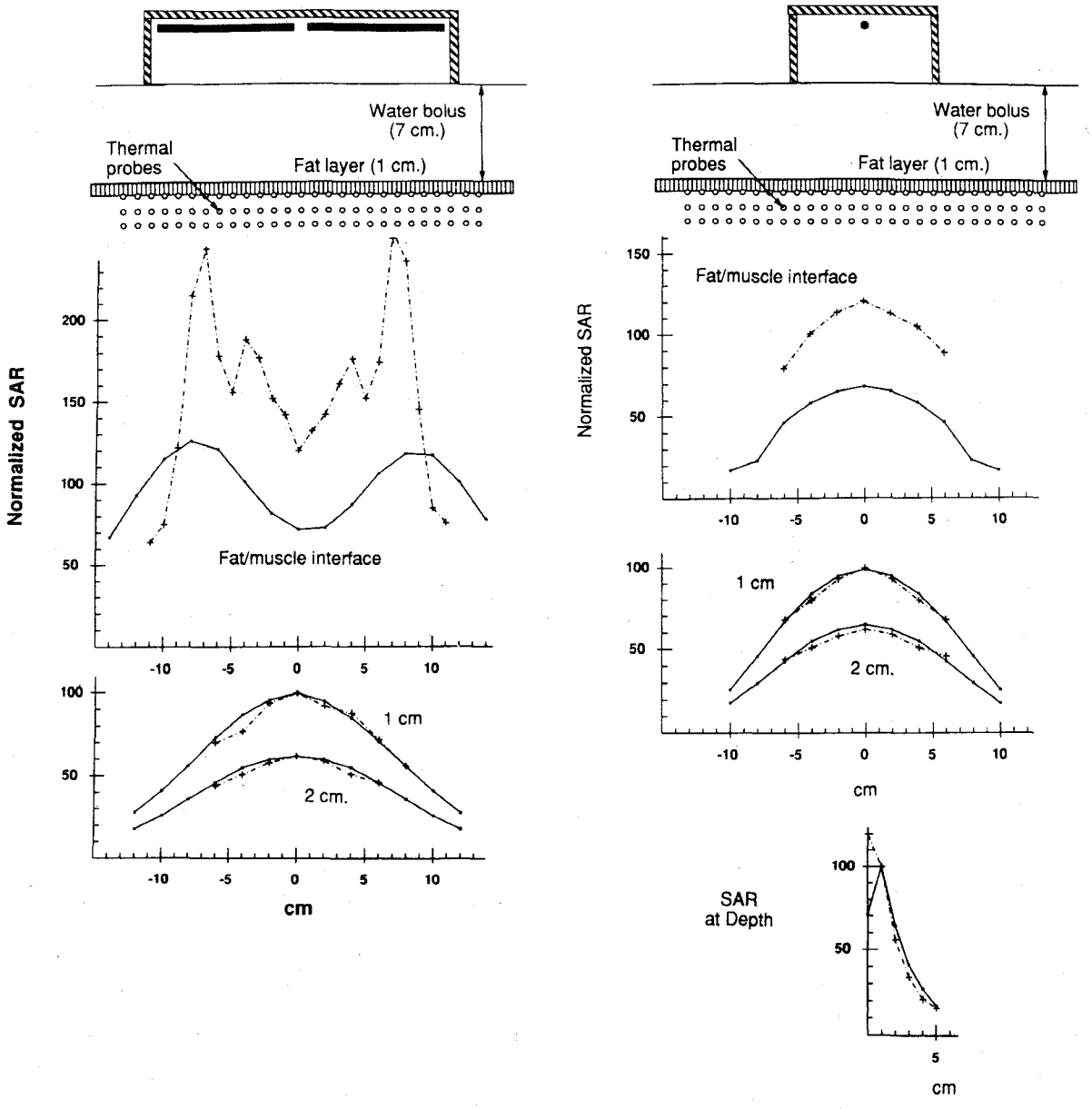


Fig. 3. FDTD versus measured *SAR*'s for a 19 cm dipole applicator at 95 MHz. The applicator rests on a 7 cm water bolus which is on a 1 cm slab of fat-equivalent material on the muscle phantom. Measurements are made at the fat/muscle interface and at 1 and 2 cm depths into the phantom.

negative peaks. The phase relative to the incident $E_z$ value can then also be determined by saving the value of $n$ in (4). Note that once steady state is reached, the $H$ fields surrounding the dipole should reflect the current distribution that would be running through the arms of the dipole. Although the $H$ fields are not saved everywhere, the amplitude and phase of the $H$ field next to the dipole are stored. The reason will be discussed later.

A box containing phantom material which is approximately muscle equivalent [17] is used for device testing. This box has 16 gauge tubes running through it, through which temperature probes can be inserted. On top of the phantom is a solid slab of fat-equivalent material. Temperature probes are also located between the fat and the muscle phantom. On top of the fat is another water bolus on which the applicator is placed.

The test is conducted by using the applicator to illuminate the phantom material when the thermal probes are in place, typically for about 2 min. At the end of the test, the rate of rise in temperature is calculated to determine the *SAR*. The same problem is simulated with the FDTD method, and the *SAR* patterns are compared. These simulations require 3 to 6 min CPU time on a Cray XMP or Cray II. Normally, the *SAR* is calculated in the FDTD method by (5), which means that the *SAR* is implicitly calculated at the center of the cell. Therefore, the FDTD program would calculate the *SAR* values in the center of the fat slab, 0.5 cm into the phantom, 1.5 cm into the phantom, etc. However, for the purpose of this test, the *SAR*'s in the FDTD program were determined by averaging adjacent *SAR* values forward into the phantom. This causes the *SAR*'s in the simulation to be calculated at the

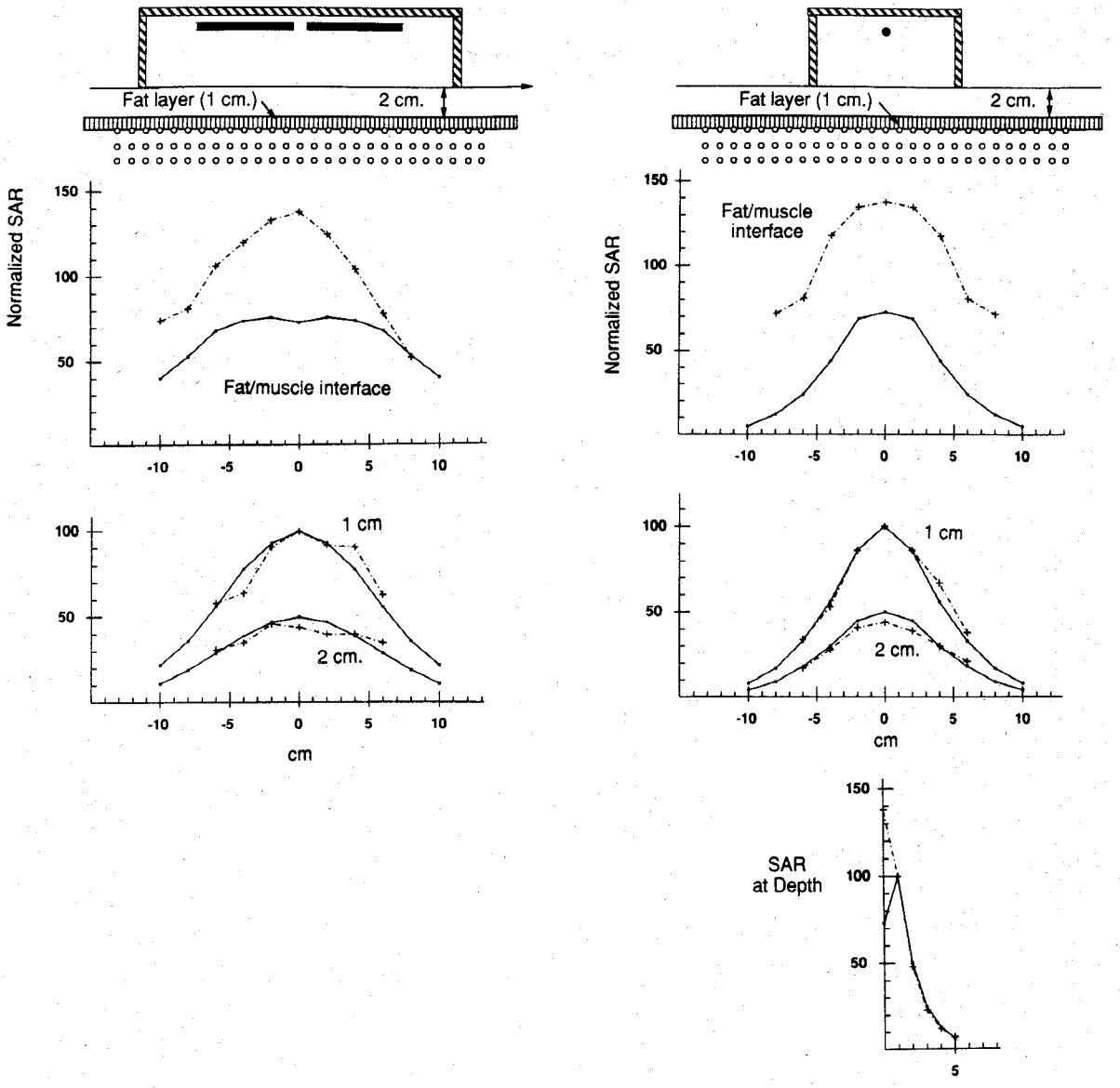


Fig. 4. FDTD versus measured *SAR*'s from a 13 cm dipole applicator at 250 MHz. The applicator rests on a 2 cm water bolus which is on a 1 cm slab of fat-equivalent material on the muscle phantom. Measurements are made at the fat/muscle interface and at 1 and 2 cm depths into the phantom.

same points they are measured, i.e., at the fat/muscle interface, at 1 cm, 2 cm, etc.

The first test was for a 19 cm dipole driven at 95 MHz. Test results are shown in Fig. 3. Since only *SAR* patterns are being tested, both the measured and calculated *SAR*'s are normalized so the *SAR* at 1 cm depth directly under the dipole is 100. Agreement within the muscle phantom is good, but there is disagreement in the magnitude at the muscle/fat interface. The lack of quantitative agreement at the interface is not surprising. The high peak *SAR*'s under the dipole are generally attributed to normal $E$ field components due to charge buildup on the end of the dipole. The severe discontinuity in dielectric constants at the fat/muscle interface causes a discontinuity in the $E$ fields. Since the resolution of the FDTD method is 1 cm, it cannot detect the full impact of this phenomenon. In this case, the problem is exacerbated because the *SAR*'s are averaged across the interface. Also, the temperature probes at this point are lying between the fat slab and the muscle phantom, giving the possibility of air gaps or other problems at this point. However, the simulation did predict the "hot spot" that appears. (Even though normal $E$ field components create errors at boundaries with severe dielectric discontinuities, the FDTD method has been shown to be capable of correct calculations on both sides of the boundary [15].)

In an effort to find a similar applicator that did not have this hot spot, simulations were run for different dipole lengths and frequencies using the same applicator housing. (The frequencies are chosen partly on the basis of available power supplies.) It was found that a 13 cm dipole driven at 250 MHz did not produce a high temperature at the interface. The comparison of simulated and measured results are illustrated in Fig. 4. Once again, the agreement at

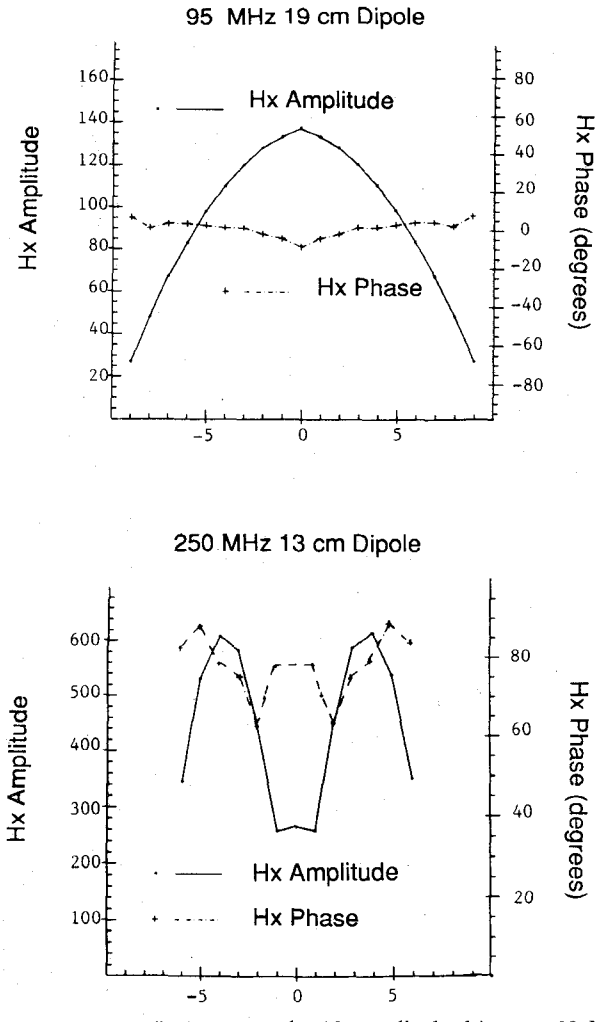


Fig. 5. Magnetic field next to the 19 cm dipole driven at 95 MHz (above), and the 13 cm dipole at 250 MHz. The magnetic field is an indication of the current through the dipole.

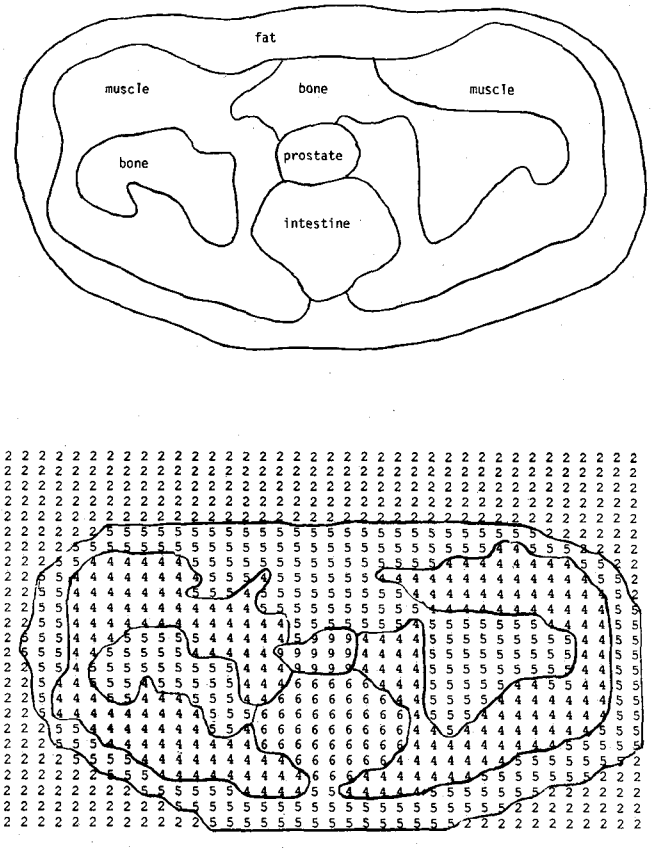


Fig. 6. Cross section at the prostate level of a cancer patient. Above is a tracing made from the CAT scan; below is the digitized version that forms the input to the FDTD program.

TABLE I
RELATIVE DIELECTRIC CONSTANTS AND CONDUCTIVITIES USED IN THE MODEL

| Number | Organ | Relative Dielectric Constant | Conductivity (S/m) |
|---|---|---|---|
| 1 | Air | 1.0 | 0.000 |
| 2 | Distilled water | 80.0 | 0.000 |
| 3 | Metal | 1.0 | 10,000,000 |
| 4 | Muscle | 73.5 | .900 |
| 5 | Fat/bone | 7.5 | 0.067 |
| 6 | Intestine | 36.2 | 0.550 |
| 7 | Liver | 77.0 | 0.620 |
| 8 | Kidney/pancreas | 90.0 | 1.000 |
| 9 | Prostate | 73.5 | .900 |

the surface is only qualitative, but it is good enough to see that the hot spot has been eliminated.

As mentioned above, the amplitude and phase of the $H$ fields next to the dipole can be determined. The tangential components of these $H$ fields are plotted for the 19 and 13 cm dipoles in Fig. 5. The tangential component of the magnetic field next to the metal arm of the dipole is an indication of the current running through the arms of the dipoles [4]. Since the incident $E$ field is known, this presents the possibility of determining the input impedance of the device being tested. Note that the 19 MHz dipole, which was driven at 95 MHz, has its $H$ field in the pattern of a classic half-wavelength dipole. The 13 cm dipole at 250 MHz has a shape closer to a full-wavelength dipole, and a more complex phase pattern. These results are preliminary, and the efficacy of using the FDTD method to determine input impedance is yet to be determined.

Thus far, using only these simple dipole antennas, no acceptable applicator for deep regional hyperthermia has been developed. At 250 MHz, electromagnetic energy is absorbed too quickly, and at 95 MHz there was a hot spot near the skin surface. Of course, the 95 MHz applicator could still be used if a larger water bolus, say 15 cm, were used to distance it from the skin surface. This would eliminate the hot spot, but at such a large distance the energy would be so dispersed by the time it reached the body that the advantage of having single discrete applicators over an APA applicator would be lost.

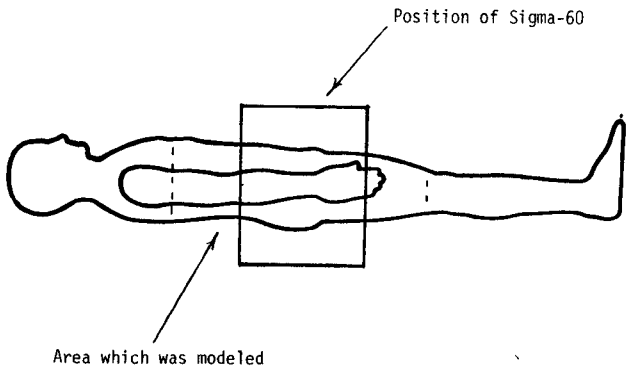


Fig. 7. Position of the applicator relative to the body. The dashed lines indicate the border of the area that was modeled for the program.

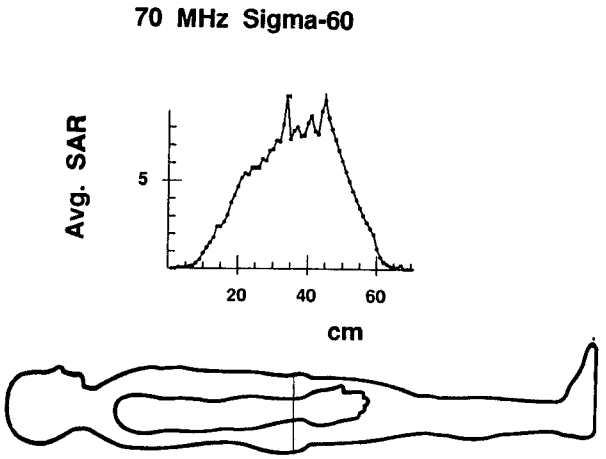


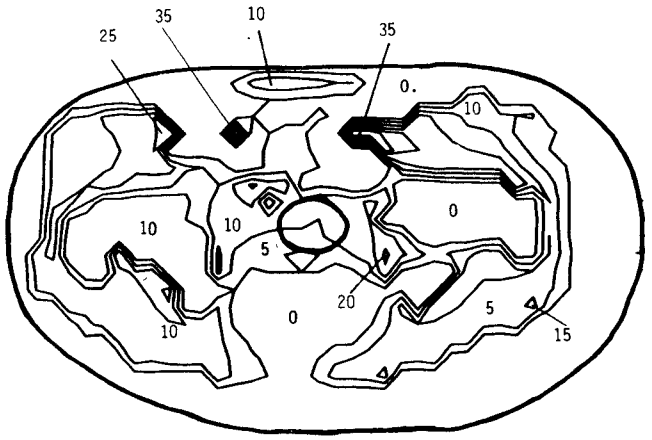


Fig. 8. Simulated treatment of a prostate cancer patient using the BSD Sigma-60 at 70 MHz. The small circle in the contour diagram indicates the location of the prostate. Contour interval is 5 W/kg. Average *SAR* in prostate = 0.518 W/kg. *SAR* in body = 0.189 W/kg. Average prostate sar/avg total = 2.74.

Clearly there are problems yet to be solved. But with the simulation techniques presented here, different antenna configurations, different dielectric interfaces, different applicator housings, and all of the parameters associated with the design can be simulated. This represents a substantial savings in time over the trial-and-error construction of new applicators.

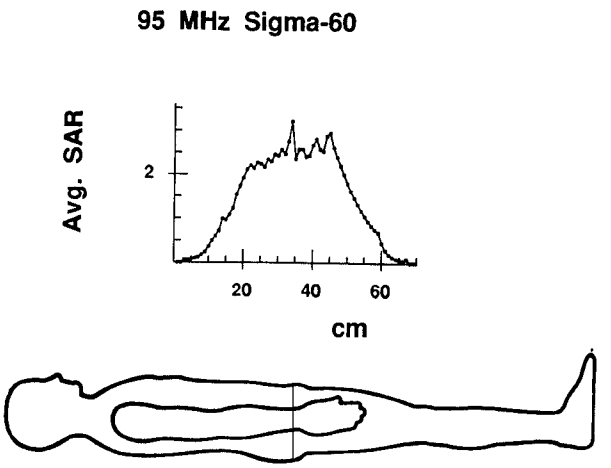


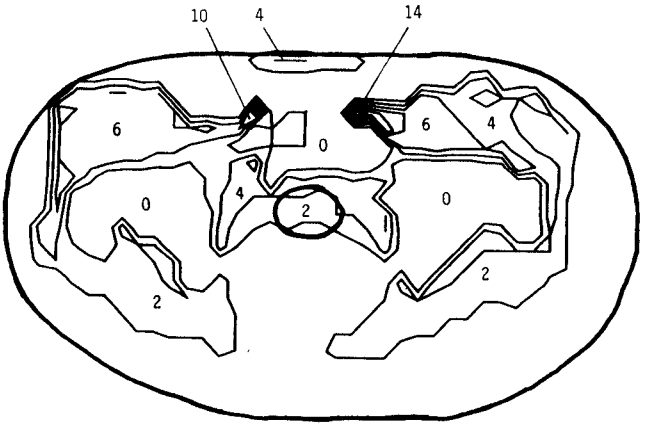


Fig. 9. Simulated treatment of a prostate cancer patient using the BSD Sigma-60 at 95 MHz. The small circle in the contour diagram indicates the location of the prostate. The contour interval is 2 W/kg. Average *SAR* in prostate = 1.86 W/kg. Average *SAR* in body = 0.63 W/kg. Average prostate sar/avg body = 2.95.

## IV. Treatment Planning

In this section, the results of using the FDTD method to predict the *SAR* distribution using the Sigma-60 applicator of the BSD-2000 Hyperthermia System will be presented. The Sigma-60 is an APA applicator which uses eight dipoles, 43 cm long, around a 60 cm diameter. The patient modeled was a 57-year-old male with prostate cancer. Fig. 6 is a diagram taken from the patient's CAT scan at the level of the prostate, and the digitized version which forms the input of the FDTD programs. The various values for the dielectric constants and conductivities of the various organs are presented in Table I [18]. Sixty-five such slices, corresponding to the area between midchest to just above the knees, form the entire input data base. Where possible, these were taken from the CAT scans. The thighs were constructed from a cross-section anatomy book [19]. Fig. 7 indicates the part of the anatomy which was modeled in comparison to the position of the Sigma-60. For these simulations, a cell size of 1 cm was used. The entire model of the patient consists of 34751 cells. The whole problem, which includes the Sigma-60 applicator, resides in a lattice with dimensions $74 \times 74 \times 80$.

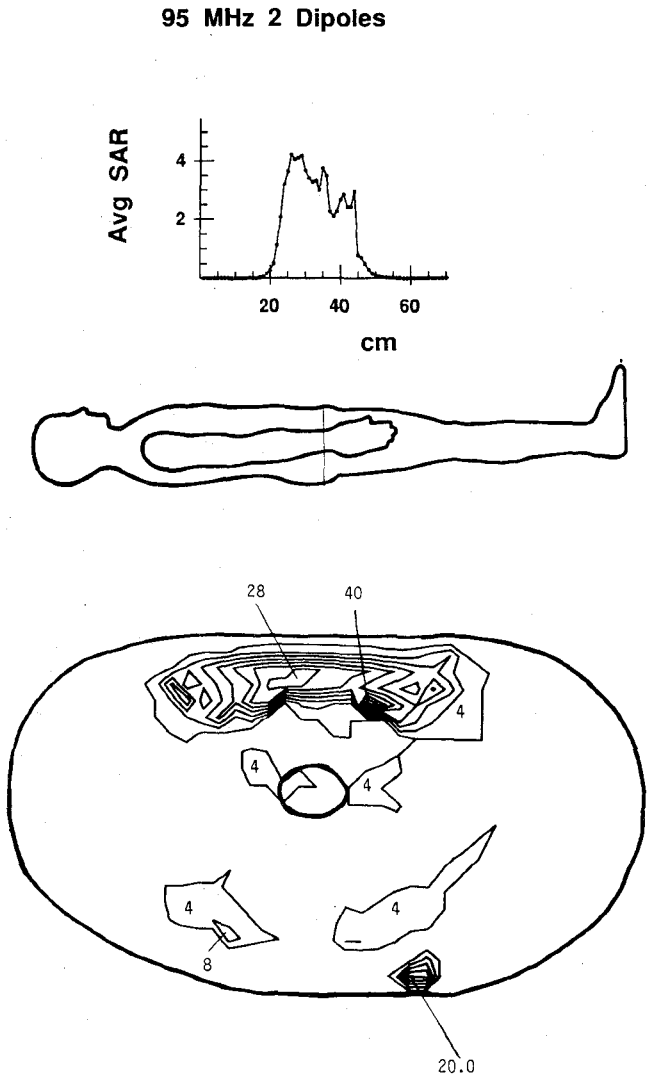


Fig. 10. Simulated treatment of a prostate cancer patient using two 19 cm dipole applicators at 95 MHz. Applicators are positioned at anterior and posterior midline centered at the level of the prostate. The small circle in the contour diagram indicates the location of the prostate. Contour interval is 4 W/kg. Average *SAR* in prostate = 1.74 W/kg. Average *SAR* in body = 0.54 W/kg. Average prostate sar/avg body = 3.24.

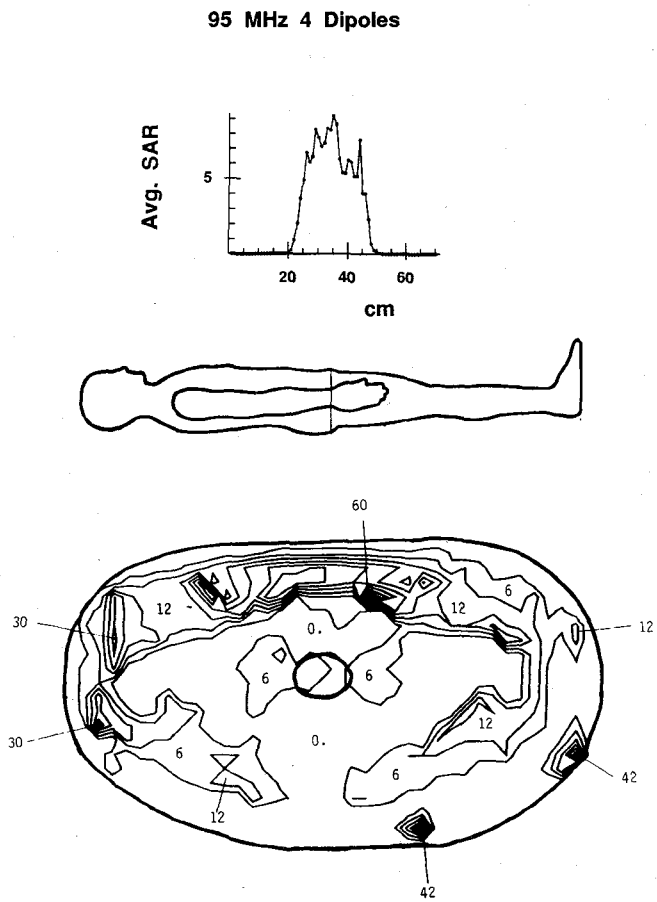


Fig. 11. Simulated treatment of a prostate cancer patient using four 19 cm dipole applicators at 95 MHz. Applicators are positioned at anterior and posterior midline, and at the hips centered at the level of the prostate. The small circle in the contour diagram indicates the location of the prostate. Contour interval is 6 W/kg. Average *SAR* in prostate = 3.09 W/kg. Average *SAR* in body = 1.12 W/kg. Average prostate sar/avg body = 2.77.

Figs. 8 and 9 show the results for runs at 70 and 95 MHz, respectively. For these runs, equal amplitudes and phases were assumed on all dipoles. The layer-averaged *SAR* profile is plotted along with the contour diagram for the layer going through the prostate. The software also calculates the total energy absorbed by the body, the energy absorbed in the prostate, and the ratio of the two. (These are listed in the captions of the figures.) Judging by this ratio, 95 MHz would be the better frequency for this treatment. Each run requires about 10 CPU min on a Cray 2 supercomputer.

The same software can be used to improve treatment planning in the following way: Successive runs can be made with only one quadrant (a group of two adjacent dipoles) activated at a time. By using the recorded phase of the $E$ field at the site being treated, e.g., the prostate, the relative phase shifts among the four quadrants can be determined to give the maximum constructive interference of the dominant $E$ field. This represents an advantage over determining phase settings by simple geometric distances, because it takes into account variations in speed of propagation from different directions due to the inhomogeneity of the body being treated.

A program similar to that used to model the Sigma-60 can simulate treatments using prototype applicators similar to the discrete dipole applicators described in the previous section. The parameters describing the applicators, the position and orientation of the applicators, and the frequency, amplitude, and phase of the excitation are set at run time. The same patient model was used. Fig. 10 shows the results using two applicators placed at the anterior and posterior midline at prostate level. These applicators contained the 19 cm dipoles and were driven at 95 MHz. The layer-averaged *SAR* indicates that the energy would be limited to a smaller area on the patient's torso. The contour diagram also shows that less normal tissue would be heated. In fact, the prostate to total body *SAR* ratio is slightly better than what was attained with the Sigma-60 simulation. However, the layer-averaged *SAR*

profile shows a peak about 8 cm above the prostate level, which is in keeping with the measured peaks under the 19 cm dipole reported in the previous sections. This, coupled with the high peak *SAR*'s in the contour, indicates that satisfactory heating of the prostate gland would not be achievable without severe hot spots at other points in the patient. For comparison, another simulation using four dipole applicators was run, adding applicators at the left and right hips at prostate level. The results in Fig. 11 do not show an advantage over the two applicators.

## V. Conclusion

The finite-difference time-domain method has been presented as a means of obtaining realistic three-dimensional modeling for deep regional hyperthermia. The ability of the method to determine *SAR* distributions for prototype applicators has been demonstrated. Efforts in the future will center on obtaining more precise measurements to determine what accuracy can be expected, and to quantifying the results, i.e., determine the magnitude of *SAR*'s for a given input, as opposed to relative *SAR* patterns. It is also believed that the FDTD method can determine the input impedance of a simulated applicator, but this is yet to be determined. Such simulation techniques present an attractive alternative to the laborious process of trial and error in constructing and testing new devices.

It has also been shown that the FDTD method can handle large three-dimensional models of human patients, making it suitable for treatment planning. A model of a cancer patient has been constructed, and the ability of the method to evaluate potential treatments on commercially available equipment or with prototype applicators has been presented. Some software development remains to speed up the process of reading the input data from CAT scans. Then the ability of the method to play a role in treatment planning on the BSD-2000 Hyperthermia System can be evaluated.

## Acknowledgment

The author is grateful to Prof. A. Taflove of Northwestern University, Prof. O. Gandhi of the University of Utah, and Dr. P. Turner of the BSD Medical Corporation for several helpful discussions; to Prof. P. Fessenden for his help in preparing this manuscript and F. van den Haak for his machining skills; and to colleagues G. Hahn, D. Kapp, S. Prionas, E. Lee, A. Lohrbach, and I. Peterson for their wisdom and counseling.

## References

[1] M. F. Iskander, P. F. Turner, J. T. DuBow, J. Kao, "Two-dimensional technique to calculate the EM power deposition pattern in the human body," *J. Microwave Power*, vol. 17, no. 3, pp. 175–185, 1982.

[2] V. Sathiaseelan, M. F. Iskander, G. C. Howard, N. M. Bleehen, "Theoretical analysis and clinical demonstration of the effect of power pattern control using the annular phased-array hyperthermia system," *IEEE Trans. Microwave Theory Tech.*, vol. MTT-34, pp. 514–519, 1986.

[3] S. Mizushina, Y. Xiang, and T. Sugiura, "A large waveguide applicator for deep regional hyperthermia," *IEEE Trans. Microwave Theory Tech.*, vol. MTT-34, pp. 644–648, 1986.

[4] C. Wang and O. P. Gandhi, "Numerical simulation of annular phased arrays for anatomical based models using the FDTD method," *IEEE Trans. Microwave Theory Tech.*, vol. 37, pp. 118–126, 1989.

[5] R. W. M. Lau *et al.*, "The modeling of biological systems in three dimensions using the finite-difference method: II The application and experimental evaluation of the method in hyperthermia applicator design," *Physics in Medicine and Biology*, vol. 31, pp. 1257–1266, 1986.

[6] A. Taflove, "Review of the formulation and applications of the finite-difference time-domain method for numerical modeling of electromagnetic wave interactions with arbitrary structures," *Wave Motion*, vol. 10, no. 6, pp. 547–582, 1988.

[7] P. F. Turner, "Regional hyperthermia with an annular phased array," *IEEE Trans. Biomed. Eng.*, vol. BME-31, pp. 106–114, 1984.

[8] P. F. Turner, "Hyperthermia and inhomogeneous tissue effects using an annular phased array," *IEEE Trans. Microwave Theory Tech.*, vol. MTT-32, pp. 874–882, 1984.

[9] K. S. Yee, "Numerical solution of initial boundary value problems involving Maxwell's equations in isotropic media," *IEEE Trans. Antennas Propagat.*, vol. AP-17, pp. 585–589, 1966.

[10] G. Mur, "Absorbing boundary conditions for the finite-difference approximation of the time-domain electromagnetic field equations," *IEEE Trans. Electromagn. Compat.*, vol. EMC-23, pp. 377–382, 1981.

[11] A. Taflove, "Application of the finite-difference time-domain method to sinusoidal steady-state electromagnetic penetration problems," *IEEE Trans. Electromagn. Compat.*, vol. EMC-22, pp. 191–202, 1980.

[12] K. Umashankar and A. Taflove, "A novel method to analyze electromagnetic scattering of complex objects," *IEEE Trans. Electromagn. Compat.*, vol. EMC-24, pp. 397–405, 1982.

[13] R. Holland, "Threde: a free-field EMP coupling and scattering code," *IEEE Trans. Electromagn. Compat.*, vol. NS-24, pp. 2416–2421, 1977.

[14] A. Taflove and M. E. Brodwin, "Computation of the electromagnetic fields and induced temperatures within a model of the microwave-irradiated human eye," *IEEE Trans. Microwave Theory Tech.*, vol. MTT-23, pp. 888–896, 1975.

[15] D. M. Sullivan, D. T. Borup, and O. P. Gandhi, "Use of the finite-difference time-domain method in calculating EM absorption in human tissues," *IEEE Trans. Biomed. Eng.*, vol. BME-34, pp. 148–156, 1987.

[16] D. M. Sullivan, O. P. Gandhi, and A. Taflove, "Use of the finite-difference time-domain method in calculating EM absorption in man models," *IEEE Trans. Biomed. Eng.* vol. BME-35, pp. 179–185, 1988.

[17] A. W. Guy, "Analyses of electromagnetic fields induced in biological tissues by thermographic studies on equivalent phantom models," *IEEE Trans. Microwave Theory Tech.*, vol. MTT-19, pp. 205–214, 1971.

[18] M. A. Stuchly and S. S. Stuchly, "Dielectric properties of biological substances-tabulated," *J. Microwave Power*, vol. 15, pp. 19–26, 1980.

[19] W. J. Bo, I. Meschan, and W. A. Krueger, *Basic Atlas of Cross-Sectional Anatomy*. Philadelphia: W. B. Saunders, 1980.

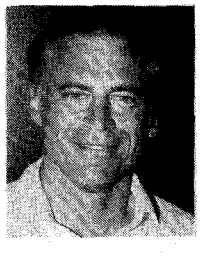

**Dennis Sullivan** received the B.S. degree in electrical engineering from the University of Illinois. He then received the M.S. degree in electrical engineering in 1978, the M.S. degree in computer science in 1980, and the Ph.D. degree in electrical engineering in 1987 from the University of Utah.

He is working on applications of computer simulation for microwave and radio-frequency hyperthermia cancer therapy at Stanford University School of Medicine, Stanford, CA, until he can resume his acting career.